UC Davis
UC Davis Previously Published Works

Title
Structural changes during the reaction of Ni thin films with (100) silicon substrates

Permalink
https://escholarship.org/uc/item/56p736md

Journal
Acta Materialia, 60(6)

Authors
Thron, Andrew M.
Greene, Peter K.
Liu, Kai
et al.

Publication Date
2012-03-05

Peer reviewed

eScholarship.org Powered by the California Digital Library
University of California

Available online at www.sciencedirect.com
SciVerse ScienceDirect
Acta Materialia 60 (2012) 2668–2678
Acta MATERIALIA
www.elsevier.com/locate/actamat

Structural changes during the reaction of Ni thin films with (1 0 0) silicon substrates

Andrew M. Thron [a], Peter K. Greene [b], Kai Liu [b], Klaus van Benthem [a,*]

[a] *Department of Chemical Engineering and Materials Science, University of California, Davis, CA 95616, USA*
[b] *Department of Physics, University of California, Davis, CA 95616, USA*

Received 6 October 2011; received in revised form 21 January 2012; accepted 23 January 2012
Available online 5 March 2012

Abstract

Ultrathin films of nickel deposited onto (1 0 0) Si substrates were found to form kinetically constrained multilayered interface structures characterized by structural and compositional gradients. The presence of a native SiO_2 on the substrate surface in tandem with thickness-dependent intrinsic stress of the metal film limits the solid-state reaction between Ni and Si. A roughly 6.5 nm thick Ni film on top of the native oxide was observed regardless of the initial nominal film thickness of either 5 or 15 nm. The thickness of the silicide layer that formed by Ni diffusion into the Si substrate, however, scales with the nominal film thickness. Cross-sectional in situ annealing experiments in the transmission electron microscope elucidate the kinetics of interface transformation towards thermodynamic equilibrium. Two competing mechanisms are active during thermal annealing: thermally activated diffusion of Ni through the native oxide layer and subsequent transformation of the observed compositional gradient into a thick reaction layer of $NiSi_2$ with an epitaxial orientation relationship to the Si substrate; and, secondly, metal film dispersion and subsequent formation of faceted Ni islands on top of the native oxide layer.
© 2012 Acta Materialia Inc. Published by Elsevier Ltd. All rights reserved.

Keywords: TEM; EELS; Thin film; Wetting; Dewetting

1. Introduction

As device sizes continually decrease, the structural and chemical stability of thin films and their properties become critical. Numerous studies have investigated thin transition metal silicide films due to their ability to form low resistance interfaces for interconnects or Schottky barriers in transistors [1,2]. Recent attention has shifted to Ni silicide as a replacement for $CoSi_2$ as interconnects, due to its lower resistivity at smaller dimensions, uniform planar growth and lower Si consumption [3]. The formation of Ni silicide is a complex process, and films have been found to be unstable as their thickness decreases [4]. Thin films of Ni silicides form by sequential growth, i.e. follow Kidson's model for planar thin film growth by solid state diffusion [5,6]. According to the binary phase diagram for Ni and Si, several intermetallic phases are stable as bulk materials; of these, Ni_2Si forms first due to the low kinetic barrier at the Ni_2Si/Si interface [6]. However, the stability of bulk phases does not necessarily reflect the structural and compositional stability in ultrathin films due to effects of intrinsic and interfacial strain, as well as the increased significance of surface and interface energies. Upon room temperature deposition of ultrathin films of Ni onto clean (1 0 0) Si substrates, nickel diffuses interstitially into the substrate [7–9]. Electrical characterizations of Schottky barrier heights have revealed that an $NiSi_2$-like "phase" is formed at the Ni–Si interface. Ni was found in solid solution, with no alterations to its diamond cubic crystal structure [7–9]. A lowering of the Schottky barrier height was explained by Si–Si covalent bonds being partially replaced by metallic Si–Ni bonds in the diffusion layer. Such observations are consistent with silicide formation at lower

* Corresponding author. Tel.: +1 530 752 5117; fax: +1 530 752 1031.
E-mail address: Benthem@ucdavis.edu (K.van Benthem).

1359-6454/$36.00 © 2012 Acta Materialia Inc. Published by Elsevier Ltd. All rights reserved.
doi:10.1016/j.actamat.2012.01.033

temperatures than predicted by the bulk phase diagram [7]. However, the formation of concentration gradients [10] resulting from reaction-limited growth was not considered, and may significantly alter the macroscopically observed Schottky barrier height.

For room-temperature deposition, compositional gradients were observed to form for monolayer thick films of Ni on (1 0 0) Si, with a diffusion layer rich in Ni near the top of the film and an Si-rich layer close to the Si substrate [11]. For film thicknesses below 2 nm, $NiSi_2$ was observed to form at temperatures as low as 350 °C through interstitial diffusion of Ni in Si and subsequent minimization of the lattice strain [11,12]. Gösele and Tu [5] and d'Heurle and Gas [6] have shown that Ni_2Si and NiSi can form simultaneously through supply-limited growth of the silicide film due to impurities at the Ni/Si interface. The incorporation of oxygen at the Ni/Si interface can, however, delay any solid-state reaction between film and substrate. Mayer and co-workers [13] have shown that a continuous layer of thermal SiO_2 with a thickness as small as 5 Å acts as a diffusion barrier for Ni below 700 K. At higher temperatures, however, Pretorius et al. [14] found that Ni films react with underlying SiO_2 by forming voids in the oxide through which the metal can diffuse to the SiO_2/Si interface and from silicide layers. Another study reports that, independent of the quality (i.e. stoichiometry) of the SiO_2 film, no diffusion of Ni through the oxide occurs below 800 °C [15]. Lee et al. [15] mostly rely on X-ray diffraction, Auger spectroscopy and transmission electron microscopy (TEM) imaging. Their TEM results, however, indicate straining at the Si/SiO_2 interface that may be caused by silicide formation after Ni diffusion through the native oxide film during rapid thermal annealing. Liehr and co-workers [16] report that, in the presence of SiO_2 diffusion barriers, solid-state reactions between Ni and Si at or above 900 °C are limited by Ni diffusion through pinholes in the oxide film. At such high temperatures, the activation energy for Ni diffusion is further lowered by complementary decomposition of SiO_2, which generates defect-rich areas and, hence, preferential diffusion pathways. Clearfield et al. [17] have demonstrated that, upon annealing, as-deposited CuNi films both dewet the Si substrate and react with the substrate to form silicides through reaction-limited diffusion across the interface plane. The authors mention that a native SiO_2 layer is present on the substrate surface. However, the presence of a possible diffusion barrier and the resulting interface reactions and their kinetics are not considered.

Another aspect that should be considered is that Ni films deposited on SiO_2 carry an intrinsic stress, which scales with film thickness [18–20]. Thin films of Ni on SiO_2 are kinetically constrained after low-temperature growth and agglomerate when annealed at or above 200 °C [13,17,21–23]. Film dispersion occurs through thermal grooving at the grain boundaries of the metal film, and is kinetically driven by surface diffusion of Ni away from the grain boundaries [24]. For nominal film thicknesses below 5 nm, the formation of a wetting layer was observed between the agglomerated Ni islands and the SiO_2 substrate acts as diffusion barrier [18,22]. Boragno et al. [22] suggest that the wetting layer forms because films thinner than 5 nm fail to reach a critical curvature, which would provide a sufficient driving force for the nucleation and growth of voids in the thin metal film. Intrinsic stress in thin metal films changes the local chemical potential and may contribute an additional driving force for Ni diffusion through an underlying SiO_2 film [20].

As-deposited thin films of Ni on Si substrates have a strong driving force for solid-state reactions to form Ni silicides through reaction-limited diffusion while reducing the intrinsic stress. Interfacial stresses have so far only been considered for silicidation processes in the absence of any diffusion barriers [19]. The literature overview provided above indicates that ultrathin stoichiometric SiO_2 films act as excellent diffusion barriers below about 800 °C [13–16,23]. However, sub-stoichiometric oxide films, such as native SiO_2, may be characterized by significantly lower activation energies for metal diffusion through the oxide layer [15,17,20]. Hence, as-deposited thin films of Ni on oxide-covered Si substrates are subject to both agglomeration and solid-state reactions with the substrate. The purpose of the reported study is to investigate the reaction kinetics between ultrathin Ni films deposited on (1 0 0) Si substrate surfaces that are covered with a thin native SiO_2 film. Cross-sectional TEM was utilized to determine whether as-deposited films show any interaction with the Si substrate or reveal any concentration gradients. Two different as-deposited film thicknesses are considered to evaluate the effects of intrinsic strain on the diffusion behavior, and in situ annealing was performed to determine the kinetic pathway for the metastable interface configuration to reach thermodynamic equilibrium.

2. Experimental details

To evaluate the influence of metal film thickness on the interface structure, nickel films with nominal thicknesses of 5 and 15 nm were deposited onto the (1 0 0) surface of Si substrates by DC magnetron sputtering at room temperature. The base pressure was 1.7×10^{-8} torr and films were deposited in an atmosphere of 2 mtorr of argon using 100 and 50 W power, resulting in sputtering rates of 1.4 and 0.7 Å s^{-1}, respectively. Prior to deposition, substrate surfaces were prepared with buffered HF solution to remove any organic contaminants. The surfaces were subsequently rinsed with de-ionized water and acetone, and dried with nitrogen.

Cross-sectional TEM specimens of the as-deposited films were prepared by standard cutting, grinding, dimpling and ion-milling techniques [25]. The temperature of the specimen was carefully controlled during specimen preparation to preserve the as-deposited film. The high temperature epoxy glue used for cross-sectional preparation was cured between 100 and 110 °C (373–383 K). Samples were cooled to liquid nitrogen temperatures during

ion-beam thinning. TEM specimens are characterized in an edge-on configuration, where the ⟨1 1 0⟩ direction of the Si substrate is parallel to the optical axis of the TEM.

High-resolution TEM (HRTEM) and selected area diffraction (SAED) experiments were carried out with a JEOL 2500SE TEM/STEM instrument, operating at 200 keV. Annular dark field scanning TEM (STEM) images were acquired with an aberration-corrected JEOL JEM 2100F/Cs STEM instrument. A Gatan Quantum parallel electron energy-loss spectrometer [26] is attached to this instrument and was used to record electron energy-loss spectroscopy (EELS) line profiles across the interface structures. HRTEM and STEM images were filtered by using a Gaussian-type high pass filter to remove high-frequency noise induced by the surrounding environment [27]. All EELS data were background subtracted using an inverse power law approximation [28]. The integrated absorption edge intensities are scaled by their calculated inelastic cross-sections [28]. After a thorough characterization of the as-deposited films, in situ heating experiments were performed with a Gatan 652 double-tilt heating holder. Temperatures were manually controlled by adjusting the heating current. A thermal couple connected to the Ta cup holding the TEM sample was used to monitor the temperature of the sample.

3. Results

3.1. As-deposited film

Fig. 1a and b shows TEM and HRTEM micrographs of the as-deposited film, respectively, with a nominal thickness of 5 nm (“thinner film”). Three distinct layers labeled A′, B and C are observed in the HRTEM micrograph in Fig. 1b. The contrast on top of layer C is some residual glue that was used during specimen preparation. Layer A′ appears wavy in the direction parallel to the interface, and varies in thickness between 0.5 and 2.0 nm. A dark band of contrast is observed along the Si/A′ interface. Layer B shows a contrast pattern that is characteristic for amorphous materials with significantly brighter intensity than observed for layer A′. Layer B is continuous over extended areas of the substrate, and its thickness varies between 1.5 and 3.0 nm. Layer C reveals a polycrystalline structure, and its thickness is approximately 6.5 nm.

Fig. 2 shows TEM and HRTEM micrographs of the as-deposited “thicker film”, with a nominal thickness of 15 nm. Four distinct layers, labeled A′, A, B and C, are observed. The first layer in contact with the single-crystalline substrate (layer A′) has a thickness of 1–2 nm and reveals some crystalline order. Layer A′ reveals a localized band of dark contrast along the Si/A′ interface. The second layer, labeled A, is polycrystalline, with a thickness of roughly 5 nm and grain sizes ranging between 15 and 76 nm in the direction parallel to the interface (Fig. 2a). The third layer, labeled B, reveals significantly brighter HRTEM image contrast and a thickness that ranges between 2 and 4 nm. Layer B is discontinuous, with lengths of intermittent sections ranging between 6 and 50 nm in the direction parallel to the interface plane. The image contrast from layer B represents an amorphous structure of the layer. Layer C is polycrystalline, with a thickness of roughly 6.5 nm and similar grain sizes. The average HRTEM image contrast in layer C is comparable to that in layer A.

SAED patterns of the interface structure for the thinner film (nominally 5 nm) are dominated by the typical diffraction spots for single-crystalline Si (Fig. 3a). A ring is observed in the diffraction pattern that coincides with the (1 1 1) lattice spacing for Ni. However, no evidence for the presence of an Ni silicide phase is observed (Fig 3a). SAED patterns of the as-deposited thicker film (nominal thickness of 15 nm) indicate the polycrystalline nature of the observed layers, with nickel (1 1 1) diffraction spots in close proximity to those generated by Si (2 0 0) planes (see Fig. 3b). In addition, diffraction spots coinciding with the (6 2 8), (0 0 8), (2 4 4) and (6 2 0) lattice plane distances in Ni_2Si are observed (Fig. 3b) [29].

Fig. 4a shows a high-angle annular dark field (HAADF) image of layer A′ of the thinner film. It is observed that in

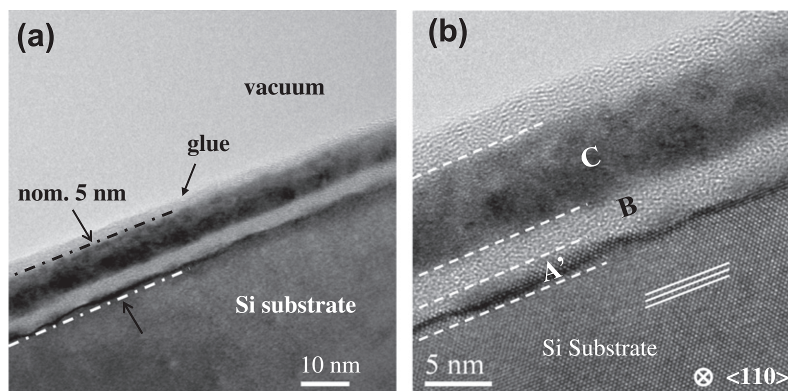

Fig. 1. TEM micrographs of the as-deposited film with a nominal thickness of 5 nm. (a) An overview of the film morphology. (b) An HRTEM micrograph displaying the formation of multiple layers, labeled A′, B and C.

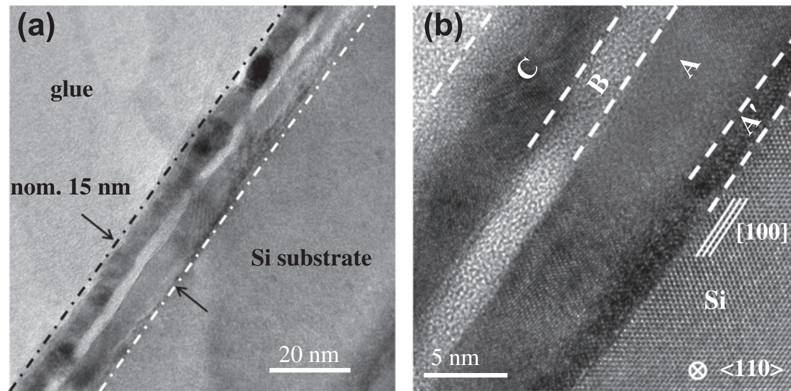

Fig. 2. TEM micrographs of the as-deposited film with a nominal thickness of 15 nm. (a) An overview of the film morphology. (b) An HRTEM micrograph displaying the formation of multiple layers, labeled A′, A, B and C.

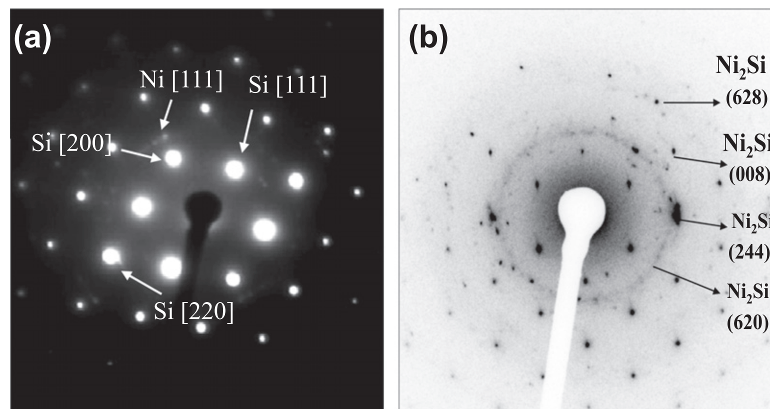

Fig. 3. SAED patterns of the as-deposited films with nominal film thicknesses of (a) 5 nm and (b) 15 nm. Only diffraction spots related to pure Ni and pure Si are observed on the thinner film, while diffraction spots corresponding to pure Ni crystals and the Ni_2Si phases are seen on the thicker film (b).

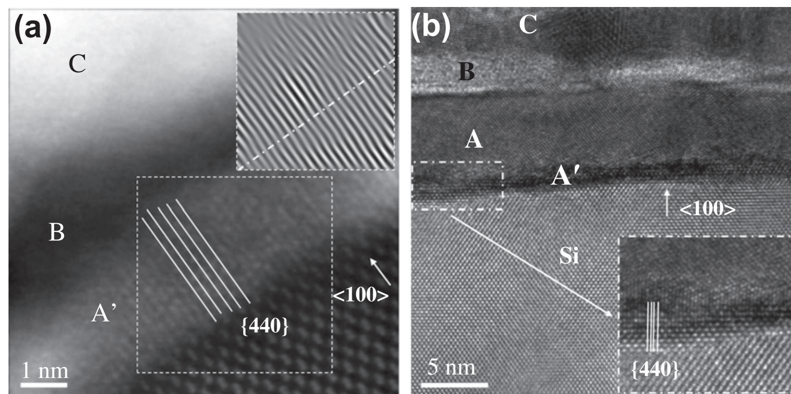

Fig. 4. (a) High-resolution HAADF image of an epitaxial section of layer A for the as-deposited thinner film. The inset is an FFT-filtered area of the highlighted area that exhibits strain due to misfit-type dislocations in the volume of layer A. (b) HRTEM image of the thicker film that in some areas reveals an epitaxial orientation relationship between layer A′ and the Si substrate (inset).

some areas lattice planes in layer A′ are aligned well with the ⟨1 0 0⟩ direction of the Si substrates. Fast Fourier transformation (FFT) of a selected area of layer A′ (see the marked area in Fig. 4a) was performed. Fourier components that represent image information in the direction parallel to the interface normal were removed from the FFT. A subsequent inverse FFT (see inset in Fig. 4a) indicates the presence of misfit-type dislocations within layer A′ that repeat in the direction parallel to the interface plane. Lattice spacings of 1.96 ± 0.20 and 2.30 ± 0.20 Å are measured below and above the dislocation lines in Layer A, respectively (see Fig. 4a). The former lattice spacing

matches well with the (440) spacing of Si in its diamond cubic structure, while the latter represents a lattice mismatch of 24% with the substrate. The epitaxial orientation relationship between layer A and the substrate as described above is, however, discontinuous along the interface plane.

Fig. 4b shows a HRTEM micrograph of the A′/Si interface for the thicker film. Layer A′ reveals a darker contrast in comparison with the other layers and formed a relatively rough, i.e. wavy, interface with the Si substrate. A lattice spacing of 1.69 ± 0.28 Å was measured in the highlighted area of the interface (inset of Fig. 4b). The observed spacing resembles the (440) spacing in the Si diamond cubic structure.

Chemical composition profiles across the as-deposited films were recorded by EELS. Profiles of the low-energy-loss and core-loss regions were acquired quasi-simultaneously using the dual-EELS technique [26]. Series of electron energy loss spectra of the Ni $L_{2,3}$, O K and Si $L_{2,3}$ ionization edges were acquired in the direction perpendicular to the substrate surface. Background subtracted spectral intensities were integrated and plotted as a function of relative distance across the interface (Fig. 4b and d). An HAADF STEM survey image of the thinner film is shown in Fig. 4a, together with the corresponding integrated EELS intensity profiles in Fig. 4b. For the thinner film, layer C is dominated by the inelastic signal from the Ni $L_{2,3}$ edge. Transitioning from layer C into layer B, the Ni signal vanishes, while the O K edge becomes dominant. Moving from the middle of layer B into layer A′, the O K edge signal drops off while the Ni $L_{2,3}$ signal gradually increases. The inelastic signal from the Si $L_{2,3}$ edge increases slightly in layer B and remains constant throughout the layer. The Si $L_{2,3}$ edge begins to increase in intensity again at the B/A′ interface, and peaks in intensity at the Si substrate. A maximum for the nickel signal occurs at the interface between layers A′ and B (top of layer A′), and gradually drops off in intensity moving into the Si substrate.

Fig. 5c shows an HAADF STEM image of the thicker as-deposited film that served as survey image during EELS acquisition. EELS intensities in layer C predominantly originate from inelastic electron scattering by nickel atoms. Entering the intermittent layer B, the Ni $L_{2,3}$ intensity reduces significantly while both the Si $L_{2,3}$ edge and the O K edge show steady increases in spectral intensity, starting at the C/B interface (the top of layer B). Layer A reveals a sharp drop in the O K edge signal at the A/B interface (the top of layer A), while the Si intensity remains mostly constant throughout both layers A and B. The Ni $L_{2,3}$ edge intensity, however, shows an abrupt increase at the top of layer A and gradually decays as it approaches the substrate. As the Ni signal decreases, the O K edge signal gradually increases when approaching the A/A′ interface (the top of layer A′). A significant increase in the Si $L_{2,3}$ edge is observed in layer A′, while the O K edge signal remains relatively constant.

Closer examination of the Si $L_{2,3}$ edge recorded from layer B for both the thinner and thicker films reveals that the observed near edge fine structures are in good agreement with reference spectra for bulk SiO_2 (Fig. 6a) [30]. The Si $L_{2,3}$ edge acquired from layer A′ in both the 5 and 15 nm films qualitatively reproduce reference spectra of bulk Si (Fig. 6b).

3.2. In situ annealing experiments

In situ heating experiments were performed while the sample was observed in cross-section by HAADF STEM imaging. Fig. 7 shows three images extracted from a video sequence that was recorded during the annealing process. The thinner films were heated from room temperature to 490 °C at a rate of 1.6 °C s^{-1}. Fig. 7a–c shows the evolution of the film for temperatures of 200, 300 and 490 °C, respectively. During the annealing of the film from room temperature to 200 °C, a reaction layer (RL) starts growing further into the substrate, while little change occurs in layers B and C. Upon further heating from 200 to 300 °C, layer C begins to disperse, as can be inferred from the area highlighted by the white oval in Fig. 8b. At 300 °C layer B remains mostly unchanged, while the RL continues to consume the Si substrate. The RL is discontinuous throughout the length of the film (cf. the dashed box in Fig. 7b). Upon heating to 490 °C, the dispersion of layer C and subsequent agglomeration into individual islands is observed (Fig. 7c). Furthermore, the newly formed RL has further consumed the Si substrate and reveals some faceting of interface with the substrate. The thickness of the RL becomes inhomogeneous, with its thinnest areas underneath larger Ni islands (cf. Fig. 7c).

A similar behavior of film dispersion and subsequent agglomeration was observed for the thicker film, although at slightly higher temperatures. The nominally 15 nm thick film was heated from room temperature to 575 °C at an average heating rate of 0.1 °C s^{-1}. Around 330 °C the Ni film starts dispersing (Fig. 7d) and continues to agglomerate (409 °C, Fig. 7e) until it shows individual islands on the amorphous film above 510 °C (see Fig. 7f recorded at 575 °C). For example, the area encircled in Fig. 7e exhibits the formation of a ridge that indicates the microstructural evolution of the metal film during annealing. At the same time, successive growth of an RL with bright image contrast was observed. Fig. 7f shows significant curvature of the interface between the RL and the substrate as well as onsets of interface faceting.

The majority of dispersed islands that formed from the thinner film reveal round edges, as shown in Fig. 8a and b. HRTEM images of the islands reveal lattice fringes spaced 2.03 Å apart, i.e. the (111) lattice spacing in metallic nickel. After annealing, the islands have thicknesses between 7.5 and 15.5 nm and widths ranging from 11 to 30 nm. The amorphous layer B remains continuous after annealing, and reveals rough interfaces with both the Ni islands and the RL.

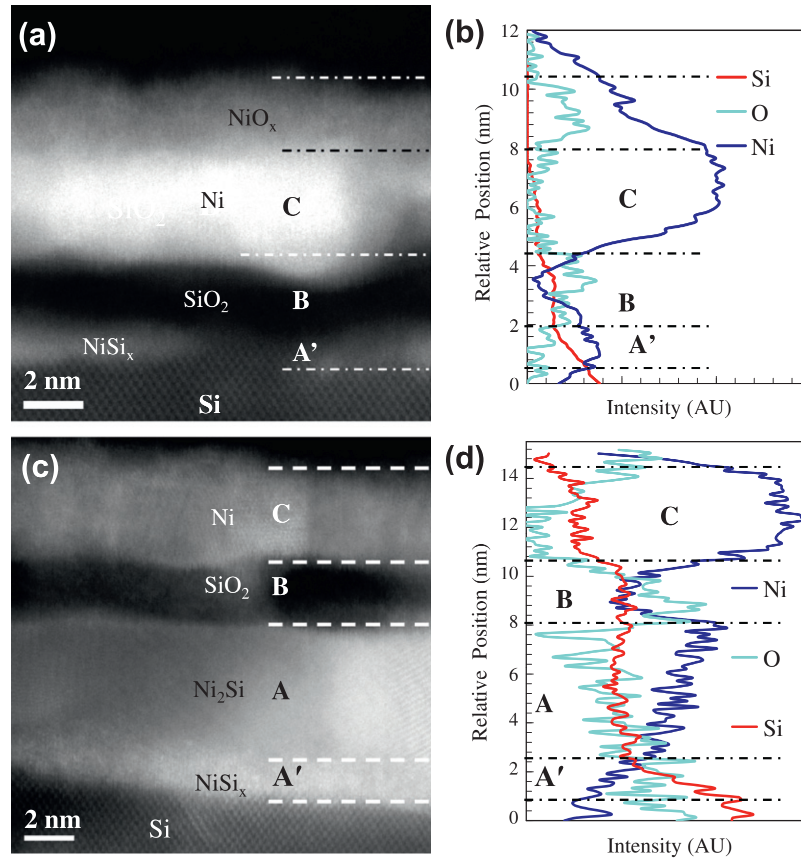

Fig. 5. Annual dark field images of the as-deposited interface structures of the nominally 5 nm (a) and 15 nm thick films (c). (b) and (d) are plots of integrated EELS intensities for the Ni $L_{2,3}$, O K and Si $L_{2,3}$ edges as a function of relative position across the interface structures shown in (a) and (c), respectively.

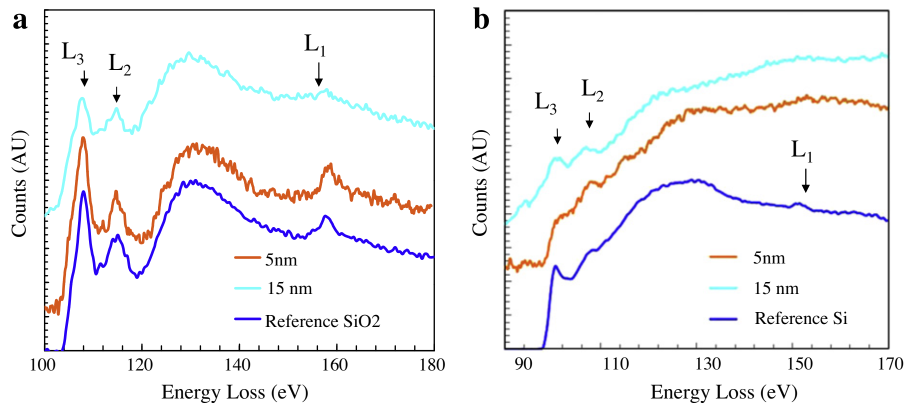

Fig. 6. (a) Si $L_{2,3}$ edge recorded from layer B of the nominally 5 and 15 nm thick films in comparison to a reference spectrum for bulk SiO_2 [41]. (b) Si $L_{2,3}$ edges recorded from layers A′ of both the 5 and 15 nm thick films in comparison to a reference spectrum for bulk Si [41].

HRTEM micrographs recorded from the thicker film after annealing (Fig. 8c and d) reveal that the previously observed ultrathin layer A′ is removed. Layer B remained amorphous and, within the field of view, became continuous in the direction parallel to the substrate surface, with thicknesses ranging between 2 and 4 nm. Similar to the thicker film, layer B exhibits rough interfaces with the adjacent islands and the RL. The coalesced nickel film (layer C) in Fig. 8d reveals small islands approximately 8–10 nm thick and 10–14 nm wide. Faceting of the nickel islands occurred along the ⟨111⟩, ⟨100⟩ and ⟨211⟩ directions (Fig. 8d). However, the nickel islands reveal a curved shape at the interface between the nickel islands and the underlying amorphous layer C. Furthermore, (100) planes of the nickel islands exhibit a small mis-tilt with respect to the (100) planes of the underlying RL.

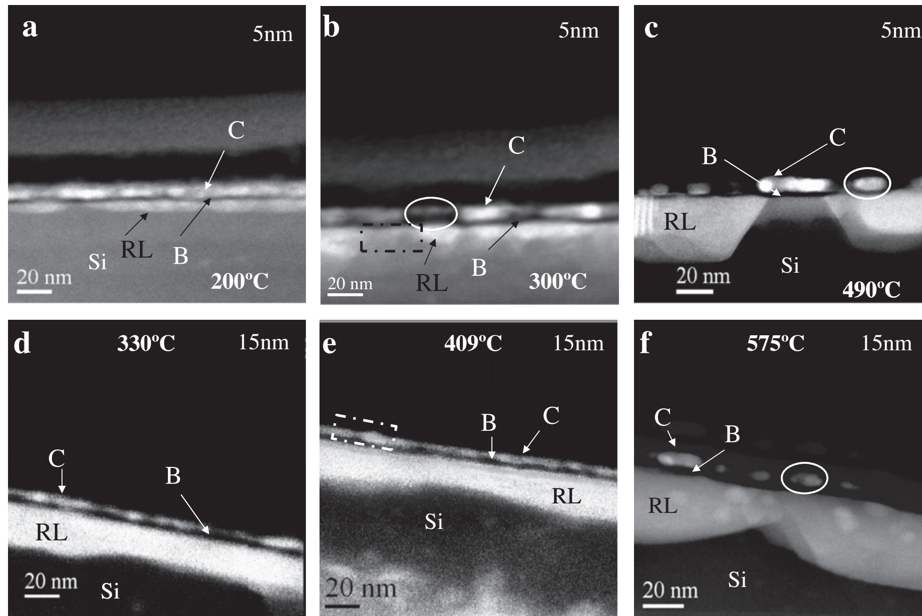

Fig. 7. Cross-sectional HAADF STEM images extracted from video clips that were recorded during the annealing of the nominally 5 nm (a–c) and 15 nm thick films (d–f). The thinner film initiates dispersion at lower temperature than the thicker film.

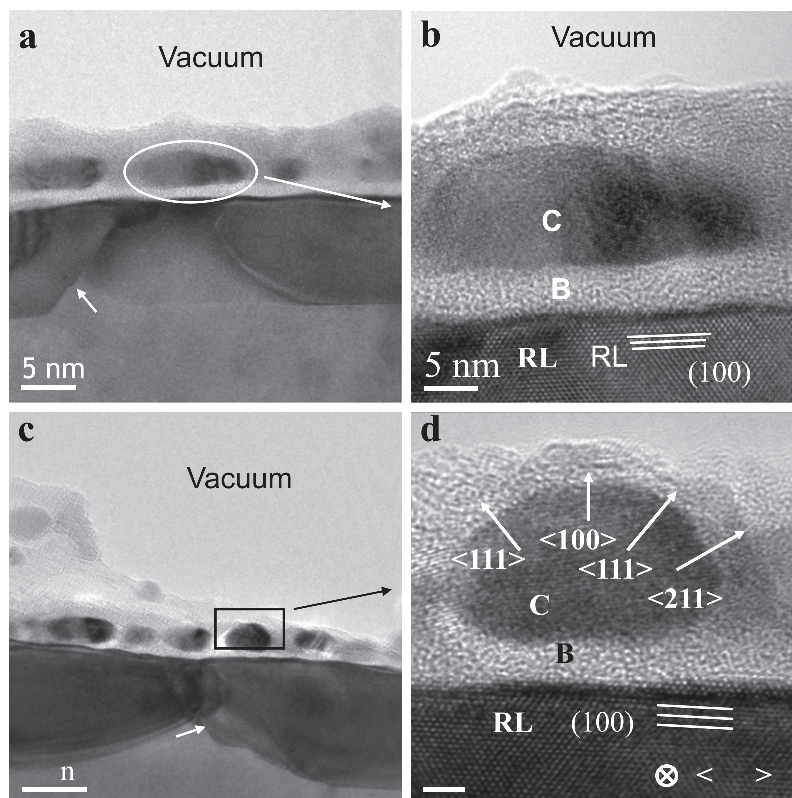

Fig. 8. (a, b) HRTEM images of dispersed Ni islands after annealing of the nominally 5 nm thick film. (c, d) HRTEM images of dispersed Ni islands after dispersion of the nominally 15 nm thick film. (d) An Ni island with four different facets.

Fig. 9 shows atomic resolution HAADF images of two different facets that are part of the interface between the RL and the Si substrate after annealing of the thinner film. The RL has an epitaxial orientation relationship with the Si substrate and forms coherent interfaces along (1 0 0) and (1 1 1) facets (Fig. 9a and b, respectively). A model of the interface, created in CrystalMaker, is overlaid at the interface on the left-hand side of Fig. 9b, confirming a coherent

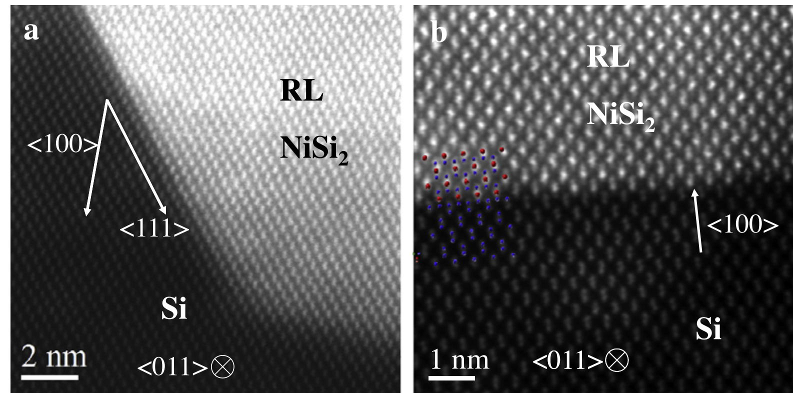

Fig. 9. Atomic resolution HAADF STEM images of {1 0 0} (a) and {1 1 1} (b) facets observed along the layer A/substrate interface after thermal annealing of the nominally 5 nm thick film. In (b) a crystal model of an $NiSi_2$/Si interface is overlaid on the left side of the image.

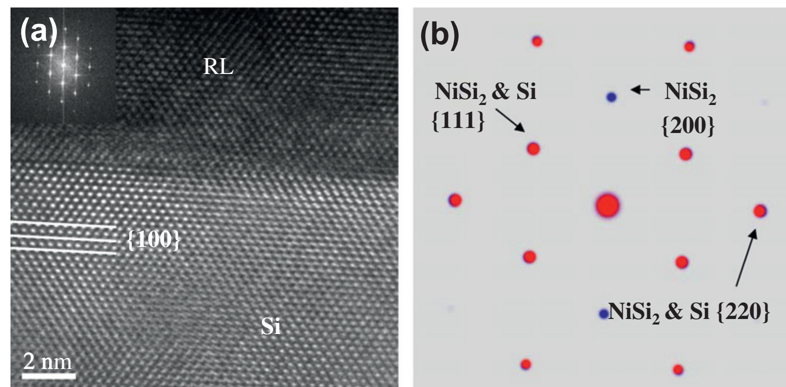

Fig. 10. (a) HRTEM micrograph of the RL/substrate interface structure after thermal annealing. The inset is a calculated FFT of the HRTEM micrograph representing the corresponding diffraction pattern. (b) A superposition of kinematically simulated diffraction patterns for bulk Si and $NiSi_2$ with the same relative orientation as observed in (a).

interface structure. Similar observations of atomically abrupt interface structures between the RL and the substrate were carried out in some areas of the thicker film after annealing (see e.g. Fig. 10a). The inset in Fig. 10a shows an FFT of the HRTEM image. Fig. 10b shows superimposed kinematically simulated diffraction patterns in $\langle 1\,1\,0 \rangle$ zone axis orientation for Si and $NiSi_2$ crystallizing in the CaF_2 structure [31].

4. Discussion

4.1. As-deposited films

For both nominal film thicknesses, multilayered interface structures were observed before any annealing was carried out. The corresponding structural and compositional gradients discussed in the following are thus formed due to the thermodynamic conditions during room-temperature deposition. It needs to be recognized, however, that the effective temperature that determines the thermodynamic condition of the observed interface structure is not room temperature. The plasma utilized during magnetron sputtering can heat the substrate surface to temperatures in excess of 100 °C, depending on the distance from the wafer to the sputtering target and the power used. In a previous study, thin metal films were successfully sputter deposited onto polycarbonate membranes under the same experimental conditions applied for this investigation. Since plastic flow of such membranes was not observed but typically occurs around 150 °C, it is concluded that the Si substrate temperature during film deposition was lower than 150 °C. During cross-sectional TEM specimen preparation, maximum temperatures of 110 °C were reached. Hence, the thermodynamic conditions for the observed "as-deposited" interface structure correspond to an effective temperature between 110 and 150 °C. For both nominal film thicknesses the observed interface structures therefore correspond to metastable thermodynamic states and are kinetically constrained. The number of observed layers (cf. Figs. 1 and 2) and their chemical composition (cf. Fig. 5) is a function of the originally deposited amount of Ni, i.e. the nominal specimen thickness. However, comparison of Figs. 1b and 2b reveals that, irrespective of the nominal film thickness, layer C assumes a thickness of roughly 6.5 nm in both observed cases. In the following, the formation of each interface layer is discussed in detail

in the sequence from closest to the interface (layer A′) towards the top of the multilayer structure (layer C).

Regardless of the nominal thicknesses, layers A′ were found to grow partially epitaxial with the Si substrate (Fig. 4). EELS results for both interface structures reveal the presence of Ni and Si (Fig. 5), while the near edge fine structures plotted in Fig. 6b indicate that the local electronic structures, i.e. bonding configurations, are similar to bulk Si. Such observations suggest that during deposition Ni diffused into the substrate and formed layer A′ consisting of a solid solution of interstitial Ni atoms in Si, which is in good agreement with earlier results reported in the literature [7,9,32]. Layer A is observed in the nominally 15 nm thick film, but is absent for the thinner film (Figs. 1 and 2). SAED patterns (Fig. 3) show the presence of Ni_2Si diffraction spots. However, layer A is characterized by a varying Ni concentration, as determined by the EELS line profiles (Fig. 5d). It is therefore concluded that layer A in the thicker film possesses a concentration gradient between an Ni-rich silicide close to the A/B interface and an Si-rich silicide at the A′/A interface. Similar chemical gradients were predicted by Gösele and Tu [5] for the growth of Ni silicide thin films by a solid-state reaction. Since the growth of Ni silicide thin films is limited by the reaction at the interface, sequential phase formation should occur. However, for the ultrathin film (layer A) in this study, the formation of the concentration gradient is due to diffusion-limited growth for the thermodynamically metastable state assumed during low-temperature film deposition.

Layer B observed for both nominal film thicknesses is an amorphous native SiO_2 layer (see Fig. 5b and d) that grew on the Si substrate surface before the sputtering process. EELS near edge fine structures of the Si $L_{2,3}$ edge acquired from both interface structures are in excellent agreement with that of an SiO_2 reference spectrum (see Fig. 6a). Stoichiometric SiO_2 acts as an excellent diffusion barrier for Ni atoms below 800 °C. However, in the current study Ni did indeed diffuse through the native oxide layer into the Si substrate to form layers A′ and A at temperatures of the order of 110–150 °C. The Ni diffusion is therefore facilitated by a high concentration of defects in the amorphous native oxide [13,16]. Areas where the native oxide film is discontinuous (Fig. 2a) indicate the location of additional pinholes before film deposition which provided preferential pathways for Ni diffusion. However, the absence of such discontinuities in layer B for the thinner film demonstrates that Ni diffusion through the volume of the native oxide layer cannot be neglected.

During the sputtering process and sample preparation, Ni had sufficient thermal energy to overcome the activation energy for diffusion through the volume of the native oxide layer. Upon the arrival of Ni atoms at the SiO_2/Si interface, Ni-rich silicide forms during the reaction-limited growth of layer A. Subsequently, Ni needs to diffuse through the previously formed silicide, resulting in reaction-limited continuation of the growth process. The resulting compositional gradient from Ni-rich to Si-rich silicide is in good agreement with predictions by Gösele and Tu [5]. After film deposition and subsequent cooling, Ni continues to diffuse into the Si substrate and eventually stops when its thermal energy drops below the corresponding activation energy. Subsequently, source-limited growth of the silicide layer occurs at the silicide/Si interface at the expense of the Ni-rich silicide. As a result, the observed compositional gradient throughout layer A is formed. However, Ni will diffuse interstitially into Si even at room temperature [32], hence creating a solid solution of Ni in Si that leads to the formation of layer A′, as discussed above.

Thin Ni films deposited on SiO_2 possess an inherent stress that increases with increasing film thickness [20] and decreases with increasing temperature [18]. As a consequence, the nominally 15 nm thick film investigated in this study carried a higher intrinsic stress than the thinner film, resulting in a larger driving force for Ni to diffuse through the oxide layer into the Si substrate. Stress-induced diffusion of Ni was therefore terminated after a sufficient decrease of intrinsic stress with decreasing film thickness reaches an equilibrium with diminished concentration gradients through the build-up of excess nickel at the SiO_2/silicide interface. The true film thickness of the nominally 6.5 nm thick films was roughly 6–8 nm and therefore small enough that only a small amount of Ni could diffuse into the Si. The observed "equilibrium film thickness" of roughly 6.5 nm is therefore determined by balancing the intrinsic stress in the metal film and the Ni concentration at the oxide/silicide interface.

Due to insufficient thermal energy, the kinetically constrained metal film was unable to completely diffuse through the native oxide layer to form a stoichiometric nickel silicide layer. To investigate the transitions of the film and the interface structure when approaching thermodynamic equilibrium, in situ annealing during TEM observation was carried out. The results are discussed in the following section.

4.2. In situ annealing

The replacement of the multilayered interface structures observed from the as-deposited films by the formation of individual Ni islands and a thick RL provides clear evidence for the metastable nature of the interface configuration observed before annealing. Two competing transitions were observed to occur during in situ heating: the continuous growth of a silicide RL through consumption of the Si substrate by Ni atoms diffusing through the oxide layer (Fig. 7); and dispersion and subsequent agglomeration of the remaining Ni film into individual islands (Figs. 7 and 8). Previous studies have shown complete consumption of thin nickel films in contact with an Si substrate to form nickel silicides after rapid thermal annealing to 850 °C [33–35]. During the in situ annealing experiments presented in this study, the formation of $NiSi_2$ crystallizing in the CaF_2 structure occurred at 280 °C for the thinner film

and 500 °C for the thicker film. The faceting in Fig. 8 demonstrates that $NiSi_2$ grew along the ⟨1 1 1⟩ direction of the Si substrate [36]. The observed significantly lower formation temperatures for $NiSi_2$ compared to 800 °C in the bulk are due to the dimensional constraints in the ultrathin layers. Previous studies of $NiSi_2$ formation have shown temperatures of formation as low as 300 °C for an initial Ni layer thicknesses below 2.5 nm [12]. Hence, limiting the supply of Ni through the diffusion barrier of the native oxide further lowered the temperature for formation of $NiSi_2$ through supply-limited growth [5]. Considering the TEM sample geometries, a contribution of combined interface and surface diffusion of nickel atoms around the SiO_2 barrier layer cannot completely be ignored. However, such effects were considered insignificant, since volume diffusion through the oxide layer was already active at temperatures below 150 °C during film deposition. Consistent with predictions by Gösele and Tu [5], the observed formation of a pure $NiSi_2$ phase at relatively low temperatures confirms the assumed supply-limited growth conditions established by volume diffusion of Ni through the SiO_2 layer.

In situ annealing of the multilayered interface structure eliminated the compositional gradients in layer A through the formation of a homogeneous RL with $NiSi_2$ composition. Such transitions are limited thermodynamically by a nucleation barrier, which was overcome at the higher annealing temperatures [6,13]. The STEM observations of the $NiSi_2$/Si interface in Fig. 9 reveals coherent interface structures due to a minimal lattice mismatch of 0.4%. Given the relatively small volume of the silicide film due to the limited Ni supply, the contribution of the interface energy to the overall free energy is significant. Thus, the formation of a coherent interface and an epitaxial orientation relationship (Fig. 9b) are thermodynamically favorable.

A similar interface structure is seen in Fig. 10a for the thicker film. $NiSi_2$ and the Si substrate are indistinguishable in the FFT shown in the inset of Fig. 10a, i.e. they are characterized by an epitaxial orientation relationship with each other. The FFT is mostly reproduced by the superimposed kinematically simulated diffraction patterns for $NiSi_2$ and Si in Fig. 10b. However, Si {2 0 0} diffraction spots are dynamically forbidden and are therefore absent in Fig. 10b.

The competing kinetic mechanism for film transition at elevated temperatures is the dispersion and subsequent agglomeration of the metal film. Evidence of dispersion and agglomeration of the Ni film is provided by Fig. 7, where the formation of grooves and ridges in the Ni thin film (Fig. 7e) indicates grain boundary grooving, which initiates void formation and film agglomeration [24,37].

The formation of a wetting layer between the Ni film and the native oxide was not observed, as previously reported for Ni films with thicknesses below 5 nm [22]. Boragno et al. reported that the formation of voids in such films was suppressed since the necessary critical curvature cannot be reached. The ridge formation observed in Fig. 7 is likely due to the alleviation of strain in the Ni film due to diffusion through the underlying oxide. However, TEM sample geometry alleviates stress at the surface of thin TEM lamellas so that the contributions of the resulting surface diffusion to the agglomeration process cannot be ignored.

The morphology of the dispersed Ni islands after in situ annealing revealed faceting along the {1 1 1}, {1 1 0} and {2 1 1} planes. This observation is in good agreement with previous results reported in the literature [21,38,39]. Recently Meltzman and co-workers [40] have shown that {1 0 0} facets are evident for the equilibrium shape of Ni nanoparticles while {2 1 1} facets are absent. The film was only annealed for a relatively short period of time during the in situ TEM experiments, and the presence of the {2 1 1} facets therefore suggest that the corresponding nickel islands have not yet fully reached thermodynamic equilibrium. However, the thickness of the TEM sample and the presence of NiO on the surface of the metal film may cause a change in the equilibrium shape of the Ni islands [40]. The dispersed Ni islands for the annealed 5 nm film show rounded edges, with no facet formation. This observation provides further evidence that the films did not have sufficient time to reach thermodynamic equilibrium during the in situ observations.

5. Conclusions

Room-temperature magnetron sputtering of thin nickel films with nominal thicknesses of 5 and 15 nm revealed the formation of a multilayered interface configuration with up to four distinct layers. The morphology of the observed interface structures was found to be metastable and kinetically constrained. The top layer was pure Ni, followed by a native SiO_2 layer due to substrate preparation. A solid-state reaction occurred between the as-deposited Ni film and the Si substrate during low-temperature deposition and TEM specimen preparation. Nickel atoms diffused through the native SiO_2 layer and, for the nominally thicker film, formed a layer of nickel silicide with spatially varying composition from Ni-rich silicide close to the interface with the oxide to Si-rich silicide towards the substrate surface. For both film thicknesses an ultrathin solid solution of Ni and Si was formed by source-limited growth on the substrate surface.

Furthermore, the topmost layer with pure Ni composition revealed an "equilibrium thickness" between 5 and 6 nm irrespective of the amount of nickel originally deposited. It was found that the origin for this specific film thickness is the minimization of intrinsic strain with deceasing film thickness, which is balanced by an excess of Ni at the oxide/silicide interface.

In situ thermal annealing of the interface structures in the TEM was used to drive the kinetically constrained interface structures towards a more stable thermodynamic state. During annealing, two different and competing mechanisms for the film transitions were observed: sup-

ply-limited growth of $NiSi_2$, and thin film dispersion and subsequent agglomeration. No wetting layer at the Ni/SiO_2 interface was observed, which is attributed to the minimization of intrinsic stress by the diffusion of Ni through the oxide layer.

The findings of this study demonstrate that rather complex interface configurations can result from concentration gradients across the original interface between two materials, and that these are determined by the intrinsic stress of the thin film, potential diffusion barriers and the effective temperature during film deposition. The formation of structural and compositional gradients needs to be considered for low-temperature deposition of metal films on semiconductors with regard to their application as Schottky barriers or ohmic contacts.

Acknowledgements

This work was funded by the US National Science Foundation (DMR-0955638 & DMR-1008791). The authors are grateful for fruitful discussions with Subash Mahajan. We acknowledge Mr. Seth Weil for excellent specimen preparation.

References

[1] Lavoie C, d'Heurle FM, Detavernier C, Cabral C. Microelectron Eng 2003;70:144.
[2] Zhang SL, Ostling M. Crit Rev Solid State Mater Sci 2003;28:1.
[3] Chamirian O, Kittl JA, Lauwers A, Richard O, van Dal M, Maex K. Microelectron Eng 2003;70:201.
[4] Deduytsche D, Detavernier C, Van Meirhaeghe RL, Lavoie C. J Appl Phys 2005:98.
[5] Gösele U, Tu KN. J Appl Phys 1981;53:3252.
[6] d'Heurle FM, Gas P. J Mater Res 1986;1:205.
[7] Tu KN. Appl Phys Lett 1975;27:221.
[8] Chang YJ, Erskine JL. Phys Rev B 1982;26:4766.
[9] Grunthaner PJ, Grunthaner FJ, Madhukar A, Mayer JW. J Vacuum Sci Technol 1981;19:649.
[10] Cahn JW. J Chem Phys 1977;66:3667.
[11] Tung RT, Gibson JM, Poate JM. Phys Rev Lett 1983;50:429.
[12] Ikarashi N. J Appl Phys 2010;107:033505.
[13] Mayer JT, Lin RF, Garfunkel E. Surf Sci 1992;265:102.
[14] Pretorius R, Harris JM, Nicolet M-A. Solid-State Electron 1978;21:667.
[15] Lee PS, Mangelinck D, Pey KL, Ding J, Dai JY, Ho CS, et al. Microelectron Eng 2000;51–2:583.
[16] Liehr M, Lefakis H, Legoues FK, Rubloff GW. Phys Rev B 1986;33:5517.
[17] Clearfield R, Railsback JG, Pearce RC, Hensley DK, Fowlkes JD, Fuentes-Cabrera M, et al. Appl Phys Lett 2010:97.
[18] Doljack FA, Hoffman RW. Thin Solid Films 1972;12:71.
[19] Liew KP, Bernstein RA, Thompson CV. J Mater Res 2004;19:676.
[20] Winau D, Koch R, Rieder KH. Appl Phys Lett 1991;59:1072.
[21] Luber E, Olsen B, Ophus C, Mitlin D. Phys Rev B 2010;82:085407.
[22] Boragno C, Buatier de Mongeot F, Felici R, Robinson I. Phys Rev B 2009;79:155443.
[23] Dallaporta H, Liehr M, Lewis JE. Phys Rev B 1990;41:5075.
[24] Mullins WW. J Appl Phys 1957;28:333.
[25] Strecker A, Bader U, Kelsch M, Salzberger U, Sycha M, Gao M, et al. Z Metall 2003;94:290.
[26] Gubbens A, Barfels M, Trevor C, Twesten R, Mooney P, Thomas P, et al. Ultramicroscopy 2010;110:962.
[27] Dave Mitchell's DigitalMicrograph Scripting Website. <http://www.dmscripting.com/>.
[28] Egerton RF. Electron energy loss spectroscopy in the electron microscope. New York: Plenum Press; 1996.
[29] Toman K. Acta Crystal 1952;5:329.
[30] Ahn CC, Rez P. Ultramicroscopy 1985;17:105.
[31] CrystalMaker Software. <http://www.crystalmaker.com>.
[32] Cheung NW, Grunthaner PJ, Grunthaner FJ, Mayer JW, Ulrich BM. J Vacuum Sci Technol 1981;18:917.
[33] Futase T, Hashikawa N, Kamino T, Fujiwara T, Inaba Y, Suzuki T, et al. IEEE Trans Semicond Manuf 2009;22:475.
[34] Utlu G, Artunc N, Budak S, Tari S. Appl Surf Sci 256:5069.
[35] De Keyser K, Van Bockstael C, Van Meirhaeghe RL, Detavernier C, Verleysen E, Bender H, et al. Appl Phys Lett 2010:96.
[36] Chiu KCR, Poate JM, Rowe JE, Sheng TT, Cullis AG. J Appl Phys 1981;38:988.
[37] Jiran E, Thompson CV. Thin Solid Films 1992;208:23.
[38] Herring C. Phys Rev 1951;82:87.
[39] Vitos L, Ruban AV, Skriver HL, Kollar J. Surf Sci 1998;411:186.
[40] Meltzman H, Chatain D, Avizemer D, Besmann TM, Kaplan WD. Acta Mater 2011;59:3473.
[41] Ahn CC, Krivanek OL. EELS Atlas. Warrendale, PA: Gatan Inc.; 1983.